ACS central science

Research Article

Cite This: ACS Cent. Sci. 2019, 5, 153−166

http://pubs.acs.org/journal/acscii

A Selective and Cell-Permeable Mitochondrial Calcium Uniporter (MCU) Inhibitor Preserves Mitochondrial Bioenergetics after Hypoxia/Reoxygenation Injury

Joshua J. Woods,[†,‡,▽] Neeharika Nemani,[§,∥,▽] Santhanam Shanmughapriya,[§,∥] Akshay Kumar,[§,∥] MengQi Zhang,[⊥] Sarah R. Nathan,[‡] Manfred Thomas,[§,∥] Edmund Carvalho,[§,∥] Karthik Ramachandran,[#] Subramanya Srikantan,[#] Peter B. Stathopulos,[⊥] Justin J. Wilson,*[,‡] and Muniswamy Madesh*[,§,∥,#]

[†]Robert F. Smith School for Chemical and Biomolecular Engineering, Cornell University, Ithaca, New York 14853, United States

[‡]Department of Chemistry and Chemical Biology, Cornell University, Ithaca, New York 14853, United States

[§]Department of Medical Genetics and Molecular Biochemistry, Lewis Katz School of Medicine at Temple University, Philadelphia, Pennsylvania 19140, United States

[∥]Center for Translational Medicine, Lewis Katz School of Medicine at Temple University, Philadelphia, Pennsylvania 19140, United States

[⊥]Department of Physiology and Pharmacology, Western University, London, Ontario N6A 5C1, Canada

[#]Department of Medicine/Nephrology, Institute for Precision Medicine and Health, University of Texas Health San Antonio, San Antonio, Texas 78229, United States

Supporting Information

ABSTRACT: Mitochondrial Ca^{2+} ($_mCa^{2+}$) uptake mediated by the mitochondrial calcium uniporter (MCU) plays a critical role in signal transduction, bioenergetics, and cell death, and its dysregulation is linked to several human diseases. In this study, we report a new ruthenium complex Ru265 that is cell-permeable, minimally toxic, and highly potent with respect to MCU inhibition. Cells treated with Ru265 show inhibited MCU activity without any effect on cytosolic Ca^{2+} dynamics and mitochondrial membrane potential ($\Delta\Psi_m$). Dose-dependent studies reveal that Ru265 is more potent than the currently employed MCU inhibitor Ru360. Site-directed mutagenesis of Cys97 in the N-terminal domain of human MCU ablates the inhibitory activity of Ru265, suggesting that this matrix-residing domain is its target site. Additionally, Ru265 prevented hypoxia/reoxygenation injury and subsequent mitochondrial dysfunction, demonstrating that this new inhibitor is a valuable tool for studying the functional role of the MCU in intact biological models.

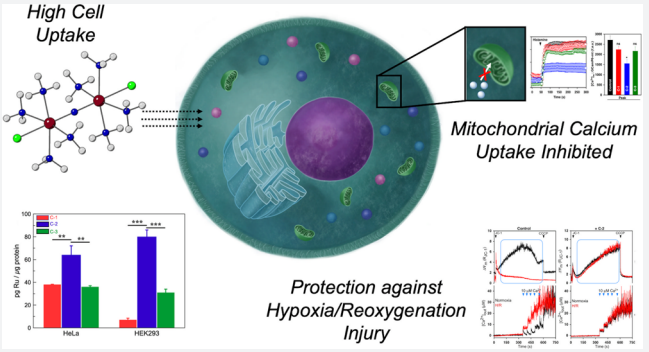

INTRODUCTION

Intracellular calcium (Ca^{2+}) ion concentration plays a crucial role in signal transduction and bioenergetics. Plasma membrane depolarization or the stimulation of receptors, such as the inositol triphosphate receptors ($InsP_3Rs$) or ryanodine receptors (RYRs), produces a transient intracellular Ca^{2+} increase. This Ca^{2+} increase is achieved by both influx from the extracellular milieu in addition to Ca^{2+} release from the endoplasmic reticulum (ER) and sarcoplasmic reticulum (SR).[1−4] Under these conditions, the highly selective and inward-rectifying Ca^{2+} channel, known as the mitochondrial calcium uniporter (MCU), acts to clear excessive cytosolic Ca^{2+}.[5−8] In this capacity, mitochondria act as Ca^{2+} sinks, shaping cytosolic Ca^{2+} ($_cCa^{2+}$) transients, while also utilizing these ions for cellular energy production.

The MCU complex comprises multiple functional domains with the MCU as the central pore-forming subunit (Figure 1A).[9−17] The MCU subunit is a 351-amino acid residue long motif with the N- and C-terminal domains both located in the inner mitochondrial matrix (IMM).[18] The transmembrane domains (TM1 and TM2) are connected through the solvent-accessible region with a highly conserved DXXE motif located in the upper helix of TM2.[19−21] The MCU pore is constructed from four of these subunits, giving a tetrameric structure.[20−23] MCU-mediated mitochondrial Ca^{2+} uptake is regulated by the proteins MCUR1,[16] EMRE,[12] MICU1,[17,24] and MICU2.[14] A 2−3 μM rise in $_cCa^{2+}$ concentration causes MICU1 and MICU2 to dissociate from the MCU, thus opening the pore

Received: October 23, 2018
Published: January 4, 2019

DOI: 10.1021/acscentsci.8b00773
ACS Cent. Sci. 2019, 5, 153−166

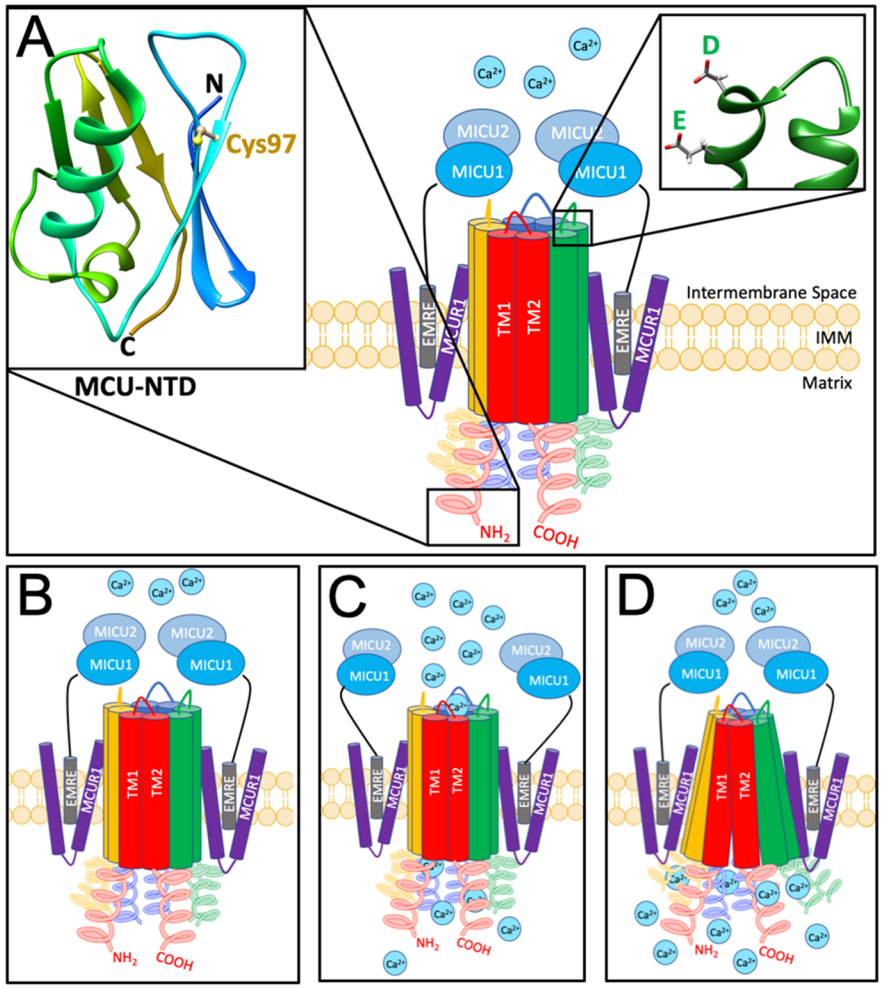

Figure 1. Topology diagram of the MCU. (A) Diagram showing the relevant regulator proteins EMRE, MCUR1, MICU1, and MICU2 and the orientation of the MCU in the IMM. Insets depict (left) the location of Cys97 in the X-ray crystal structure of the MCU-NTD (residues 72−189, PDB 5KUJ)[27] and (right) location of the DXXE motif in the solvent-accessible region of the MCU pore in the cryo-EM structure of the MCU (PDB 6DNF).[20] (B) At low Ca^{2+} concentration, MICU1 and MICU2 prevent Ca^{2+} from entering the mitochondria. (C) Elevated Ca^{2+} concentrations cause MICU1 and MICU2 to dissociate from the MCU, allowing Ca^{2+} transport across the IMM. (D) Binding of Ca^{2+} to the MRAP region in the MCU-NTD promotes a change in MCU conformation, preventing Ca^{2+} uptake.

for Ca^{2+} uptake (Figure 1B,C).[25] MCUR1, in contrast, acts as a positive regulator for $_{m}Ca^{2+}$ uptake by binding to the coiled-coil region of the N-terminal domain (NTD, residues 72−189)[26,27] within the IMM.[26,28] Like most Ca^{2+} channels, the MCU is additionally autoregulated by divalent cations such as Mg^{2+} and Ca^{2+}. Binding of divalent cations to the MCU-regulating acidic patch (MRAP) region in the β-grasp-like fold of the NTD destabilizes and shifts the self-association equilibrium of the MCU pore domain toward monomer formation. This equilibrium shift inhibits MCU function, thus fine-tuning Ca^{2+} entry into the mitochondria (Figure 1D).[27]

MCU-mediated Ca^{2+} uptake into the mitochondria is an electrogenic process that is driven by the highly negative electrochemical gradient across the IMM.[29] The surge of MCU-mediated mitochondrial Ca^{2+} ($_{m}Ca^{2+}$) uptake allosterically stimulates the mitochondrial matrix pyruvate dehydrogenase complex, α-keto-glutarate dehydrogenase, and isocitrate enzymes to generate reducing equivalents (NADH) and promote ATP production.[30−32] Although MCU-mediated mitochondrial Ca^{2+} uptake is essential for bioenergetics, Ca^{2+} overload via this pathway triggers opening of the mitochondrial permeability transition pore (mPTP), which gives rise to mitochondrial swelling and rupture, creating a cellular bioenergetic crisis and activating degradative enzymes under pathological conditions, which leads to irreversible cell damage and death.[33−36] Dysregulation of Ca^{2+} uptake by the MCU plays a major role in numerous pathological conditions such as ischemic reperfusion injury[37−39] and neurodegenerative disease.[40,41] As such, pharmacological strategies to regulate MCU activity are of great importance and may provide further insight into the role of this channel in mediating human disease.

With the significant recent interest within this field, systematic efforts to find selective and cell-permeable MCU inhibitors have only recently been initiated. However, the structural criteria required for small molecules to be effective inhibitors of the MCU is not well-established. As such, combinatorial screening strategies have recently been employed to discover organic molecules that possess MCU-inhibitory properties.[42,43] Despite the discovery of several organic small-molecule MCU inhibitors,[42−46] these compounds generally have alternative biological activities, which result in undesirable toxicity. For example, mitoxantrone was recently discovered via a combinatorial approach to be a cell-

DOI: 10.1021/acscentsci.8b00773
ACS Cent. Sci. 2019, 5, 153−166

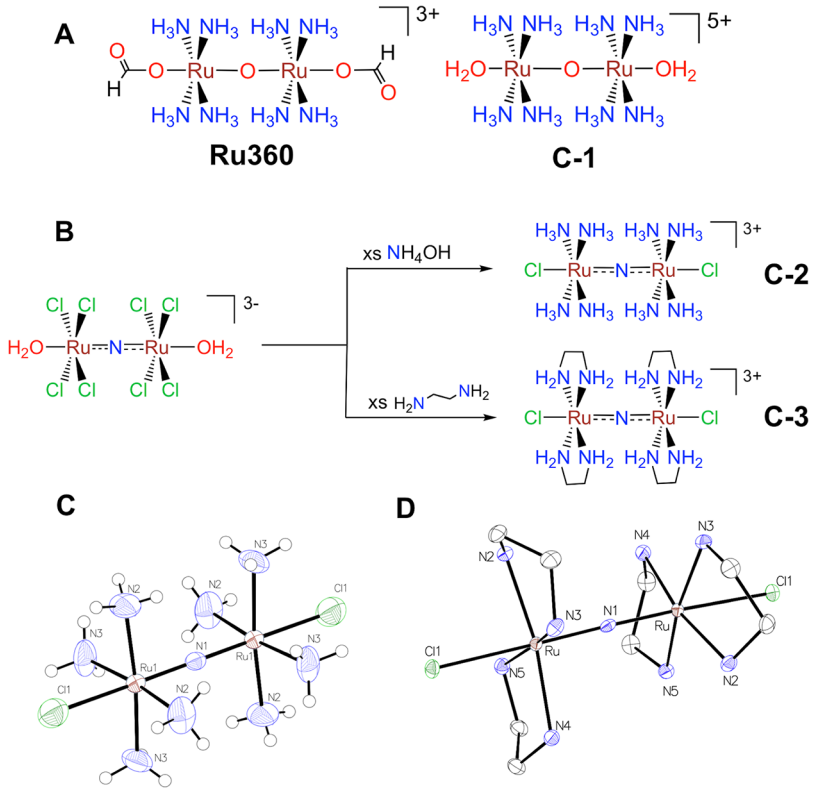

Figure 2. (A) Chemical structures of the established and commercially available MCU inhibitor Ru360 (left) and the related analogue C-1. (B) Synthetic scheme for the preparation of C-2 and C-3. Crystal structures of (C) C-2 and (D) C-3. Outer sphere chlorides and solvent are omitted for clarity. Thermal ellipsoids are shown at the 50% probability level. Interatomic distances and angles are given in Tables S1−S3 in the Supporting Information (SI).

permeable MCU inhibitor.[42] This compound, however, is an established topoisomerase II inhibitor that has been employed as a cytotoxic agent for the treatment of cancer.[47−50] In addition to these secondary biological applications, it also gives rise to cardiotoxicity,[51,52] which could hamper its in vivo applications.

The most commonly used and well-known MCU inhibitor is the inorganic binuclear oxo-bridged ruthenium complex ruthenium 360 (Ru360; Figure 2A), which was named for its strong absorbance at 360 nm. Although Ru360 is a highly potent and selective MCU inhibitor,[53−55] its widespread applicability in biological systems is limited by several factors. For example, in most cell lines, this compound is impermeant to the plasma membrane, hindering its use in intact cellular models. Furthermore, the synthesis of this complex is challenging and low-yielding,[56,57] diminishing its widespread availability. With structural data on the MCU recently becoming available, efforts to understand the mechanism of action of Ru360 have been slowly progressing. For example, site-directed mutagenesis of the S259 residue (located in the solvent exposed region of the MCU near the DXXE motif of human MCU) to an alanine gave rise to a variant of the MCU (MCU^{S259A}) that retained functional activity, but was partially resistant to the inhibitory action of Ru360.[9] This result was taken to imply that Ru360 interacts with the DXXE motif located near the central pore opening of the MCU. Additional molecular dynamics simulations and solution-state NMR studies were consistent with Ru360 interacting with aspartate residues in the DXXE motif to directly block the MCU channel.[58] Despite these initial studies, the features that give Ru360 its potency and selectivity have not been fully elucidated, thereby warranting further investigation of Ru360 and its structural analogues.

In this study, we aimed to circumvent the limitations of Ru360 by introducing structural modifications with the goal of developing synthetically available and highly potent MCU inhibitors. We have fully characterized a new ruthenium-based MCU inhibitor that is cell-permeable and have investigated its biological properties and interactions with the MCU in detail. The results described herein provide guiding principles for the design of new and effective MCU inhibitors as tools for understanding mitochondrial Ca^{2+} dynamics in intact biological systems in addition to the development of a new class of therapeutic agents.

RESULTS

Synthesis and Characterization. A key structural feature of Ru360 is its linear Ru−O−Ru functionality. We hypothesized that this Ru−O−Ru motif, a feature that is relatively unique to Ru360, is an important factor that contributes to this molecule's MCU-inhibitory activity. For example, we have previously reported on the synthesis and characterization of a very close structural analogue of Ru360 containing this motif, C-1 (Figure 2A), which is a more potent MCU inhibitor than its parent complex Ru360.[56,57] The syntheses of linear oxo-bridged transition metal complexes is not always straightforward, making it challenging to develop rational synthetic strategies.[59] Therefore, we targeted an analogous structural motif that would allow for rational synthetic strategies and facile development of new complexes.

DOI: 10.1021/acscentsci.8b00773
ACS Cent. Sci. 2019, 5, 153−166

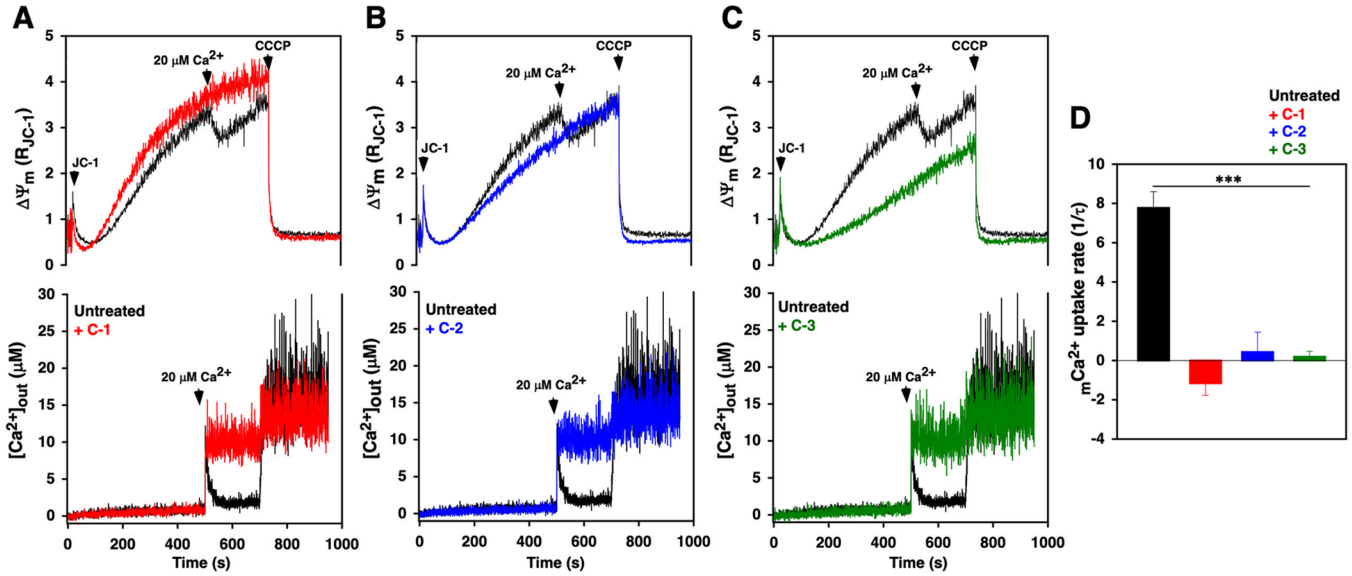

Figure 3. (A–C) Changes in $\Delta\Psi_m$ (JC-1, top panel) and extramitochondrial Ca^{2+} ($[Ca^{2+}]_{out}$) clearance (Fura-2-FF, bottom panel) in digitonin-permeabilized HEK293T cells in response to 20 μM of Ca^{2+} after treatment with 5 μM of C-1, C-2, and C-3. The transient drop in $\Delta\Psi_m$ in control cells upon Ca^{2+} addition indicates accumulation of Ca^{2+} in the mitochondrial matrix. (D) Quantification of the rate of $[Ca^{2+}]_m$ uptake as a function of decrease in $[Ca^{2+}]_{out}$ after 20 μM Ca^{2+}pulse. Data are represented as mean ± standard error of measurement (SEM); ***$p < 0.001$; $n = 3–6$.

Nitrido-bridged ruthenium complexes, which bear a structurally similar linear Ru–N–Ru core, can be readily accessed via ligand substitution reactions with the precursor complex $K_3[Ru_2(\mu\text{-}N)Cl_8(OH_2)_2]$.[60] Accordingly, the reaction of this complex anion with either aqueous ammonium hydroxide or ethylenediamine (en) afforded the expected compounds $[Ru_2(\mu\text{-}N)(NH_3)_8Cl_2]Cl_3$ (Ru265; referred to herein as C-2) and $[Ru_2(\mu\text{-}N)(en)_4Cl_2]Cl_3$ (C-3) (Figure 2B). In contrast to the low-yielding synthesis of Ru360 and related analogues, the syntheses of these compounds proceed in moderate yield and require no tedious chromatographic purification. These compounds were fully characterized by NMR, IR, UV–vis spectroscopy, and single-crystal X-ray diffraction (Figure 2, and Figure S1, Supporting Information, SI). UV–vis spectra reveal strong charge transfer bands at 265 nm (ε = 34 000 ± 2000 M^{-1} cm^{-1}) and 273 nm (ε = 29 000 ± 4000 M^{-1} cm^{-1}) for C-2 and C-3, respectively, with a lower energy shoulder observed near 325 nm for both complexes. IR spectroscopy reveals distinct bands near 1050 cm^{-1} corresponding to the asymmetric Ru–N–Ru vibrational mode. Furthermore, ^1H and $^{13}C\{^1H\}$ NMR spectroscopy showed relatively sharp signals for the NH_3 and ethylenediamine ligands, confirming the diamagnetic character of the Ru^{IV}/Ru^{IV} system.[61,62]

Single-crystal X-ray crystallography was employed to fully elucidate the three-dimensional structures of C-2 and C-3 (Figure 2C,D). X-ray diffraction quality crystals of C-2 and C-3 were grown by vapor diffusion of dioxane into water and vapor diffusion of ethanol into dilute hydrochloric acid, respectively. These structures verify the presence of both the linear Ru–N–Ru motif ($C\text{-}2_{Ru-N-Ru}$ = 180°; $C\text{-}3_{Ru-N-Ru}$ = 176.3°) and the chlorido axial ligands. Relevant interatomic distances and angles as well as details for the crystal structure refinement of C-2 and C-3 are shown in Tables S1–S3 (SI). The Ru–N distances of the nitrido bridge agree well with previously synthesized compounds.[60,63–65] The NH_3 ligands of the bridged Ru^{IV} centers of C-2 are arranged in an eclipsed configuration, whereas the ethylenediamine ligands of C-3 crystallize in a staggered conformation. This disparity may indicate that the rotation about the Ru–N–Ru axis is facile. With the new ruthenium compounds fully characterized, we proceeded to evaluate their MCU-inhibitory properties.

Mitochondrial Ca^{2+} Uptake Inhibition and Cell Permeability. With the new nitrido-bridged ruthenium compounds C-2 and C-3 in hand, we sought to evaluate their MCU-inhibitory properties and compare their activity to C-1, the oxo-bridged Ru360 analogue that we have previously reported.[56,57] We first measured the cytotoxicity of the complexes in HEK293 cells using the colorimetric thiazolyl blue tetrazolium bromide (MTT) assay.[66] This assay revealed that C-2 and C-3 are effectively nontoxic, as indicated by their IC_{50} values of 195 ± 8 and 226 ± 19 μM, respectively (Figure S2, SI). To measure the effect of these compounds on MCU activity, permeabilized HEK293T cells were treated with commercially available Ru360, C-1, C-2, or C-3 (5 μM) 200 s prior to the delivery of a 20 μM bolus of Ca^{2+} in the presence of 2 mM succinate as an energy source and the sarco/endoplasmic reticulum Ca^{2+}-ATPase (SERCA) pump blocker thapsigargin to prevent ER Ca^{2+} uptake.[67] As anticipated, extramitochondrial Ca^{2+} ($[Ca^{2+}]_{out}$) was rapidly cleared in control cells as Ca^{2+} ions were sequestered in the mitochondria by the MCU (Figure 3A). In contrast, cells that were treated with C-1, C-2, C-3 (Figure 3A–D), and commercially available Ru360 (Figure S3, SI) showed a significant reduction in MCU-mediated $_mCa^{2+}$ uptake. Additionally, the mitochondrial membrane potential ($\Delta\Psi_m$) was monitored using 5,5′,6,6′-tetrachloro-1,1′,3,3′-tetraethylbenzimidazolylcarbocyanine iodide (JC-1) dye.[68] Cells treated with commercially available Ru360, C-1, C-2, or C-3 showed no transient $\Delta\Psi_m$ loss (Figure 3A–C and Figure S3A,C, SI), a phenomenon that occurs when Ca^{2+} rapidly enters the mitochondria.[11] These results show that commercially available Ru360, C-1, C-2, and C-3 are all capable of inhibiting MCU-mediated $_mCa^{2+}$ uptake in permeabilized cells without negatively affecting the $\Delta\Psi_m$, preserving normal cell function.

DOI: 10.1021/acscentsci.8b00773
ACS Cent. Sci. 2019, 5, 153–166

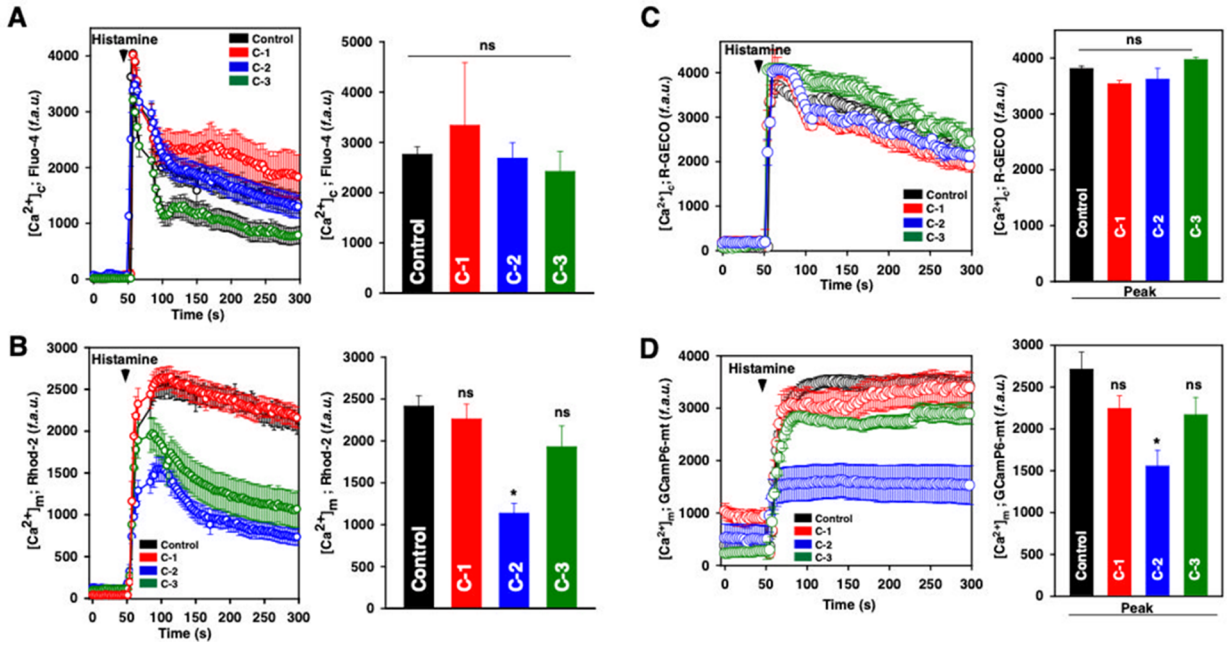

Figure 4. (A, B) Cytosolic ($[Ca^{2+}]_c$, Fluo-4 AM) and mitochondrial ($[Ca^{2+}]_m$, Rhod-2 AM) calcium transients in HeLa cells after treatment with histamine (100 μM) that were pretreated with or without C-1, C-2, or C-3 (50 μM) for 30 min. (C, D) Cytosolic ($[Ca^{2+}]_c$, R-GECO) and mitochondrial ($[Ca^{2+}]_m$, GCamP6-mt) calcium transients in HeLa cells after treatment with histamine (100 μM) that were pretreated with or without C-1, C-2, or C-3 (50 μM) for 30 min. HeLa cells were cotransfected with R-GECO1 and GCamP6-mt and analyzed 48 h post-transfection. Data are represented as mean ± SEM; $*p < 0.05$; $n = 3–6$.

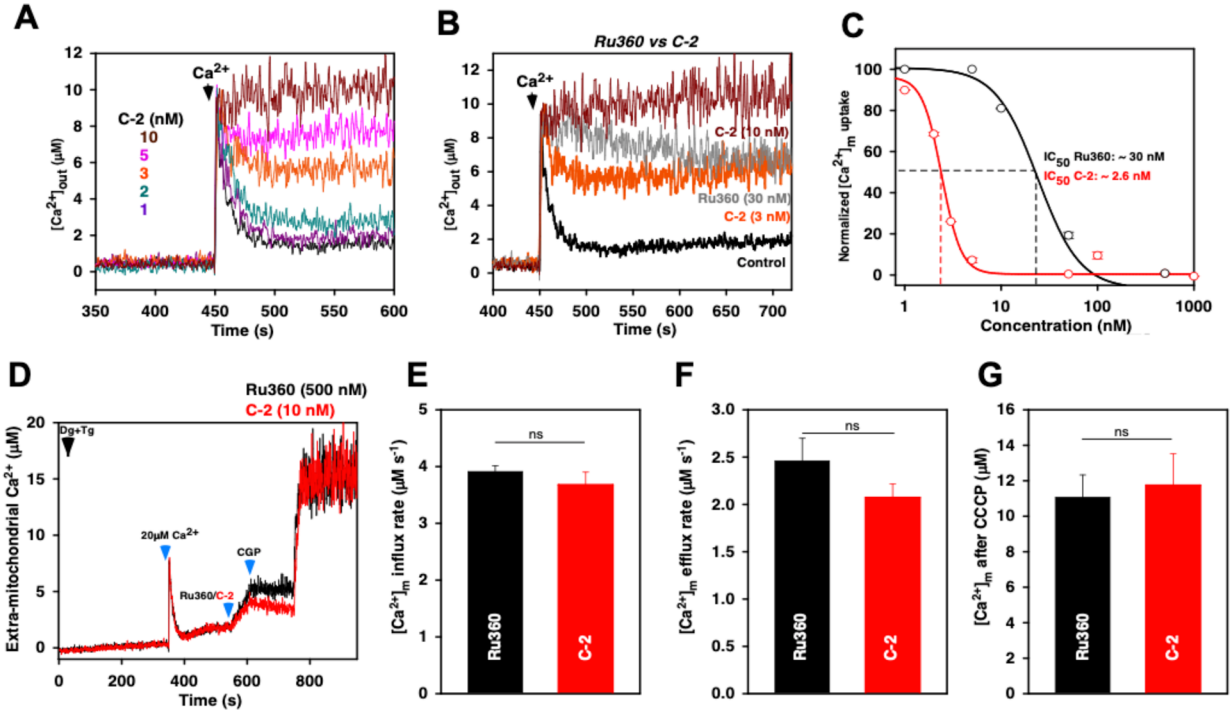

Figure 5. (A) Representative traces of $[Ca^{2+}]_{out}$ clearance in permeabilized HEK293T cells challenged with a range of C-2 concentrations (1, 2, 3, 5, and 10 nM). (B) Comparison of MCU-inhibitory effect by Ru360 (30 nM) and C-2 (3 and 10 nM) at lower concentrations. (C) Calculation of dose-dependent inhibition by C-2 and Ru360. (D) Assessment of mitochondrial Ca^{2+} influx and efflux rates. Permeabilized HEK293T cells pulsed with 20 μM Ca^{2+} at 350 s to measure mitochondrial Ca^{2+} uptake, followed by the addition of the 1 μM C-2 or Ru360 at 550 s, 10 μM CGP37157 at 600 s, and 6 μM CCCP at 750 s. Representative trace depicts the comparison of C-2 and Ru360. (E) Quantification of Ca^{2+} influx rate. (F) Quantification of Ca^{2+} efflux rate after addition of C-2 or Ru360. (G) Quantification of CCCP-induced release of accumulated mitochondrial Ca^{2+}. Data represent mean ± SEM; n.s., not significant $n = 3–6$.

We next investigated the cell permeability of the compounds and their ability to inhibit MCU activity in intact cells. The cellular uptake of C-1, C-2, and C-3 was quantified as previously described.[69,70] HEK293 or HeLa cells were

DOI: 10.1021/acscentsci.8b00773
ACS Cent. Sci. 2019, 5, 153−166

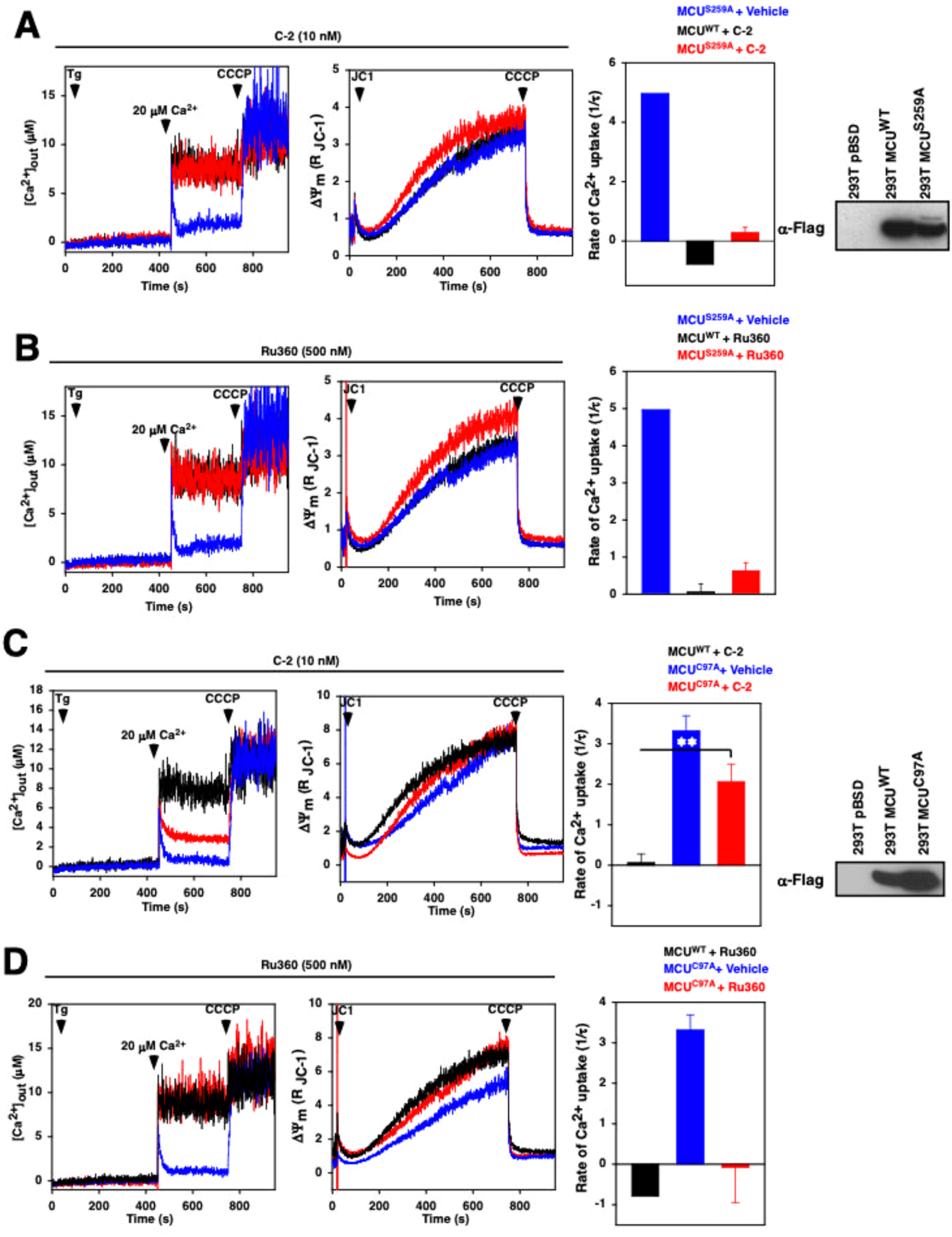

Figure 6. Representative traces of $[Ca^{2+}]_{out}$ clearance and $\Delta\Psi_m$ in permeabilized HEK293T cells stably expressing Flag-tagged MCU^{WT} and MCU^{S259A} mutant challenged with either (A) C-2 (10 nM) or (B) Ru360 (500 nM). Bar graphs represent the quantification of the rate of $[Ca^{2+}]_m$ uptake. Representative traces of $[Ca^{2+}]_{out}$ clearance and $\Delta\Psi_m$ in HEK293T cells stably expressing Flag-tagged MCU^{WT} and MCU^{C97A} mutant challenged with either (C) C-2 (10 nM) or (D) Ru360 (500 nM). Bar graphs represent the quantification of the rate of $[Ca^{2+}]_m$ uptake. Compound MCU-inhibitory effect was compared with cells reconstituted with appropriate mutants alone. Data represent mean ± SEM; ***p < 0.001; n = 3−6.; n = 4.

DOI: 10.1021/acscentsci.8b00773
ACS Cent. Sci. 2019, 5, 153−166

incubated with the complexes (50 μM) in culture media for 24 h before the cells were harvested and lysed. The amount of ruthenium in the cell lysate was determined using graphite furnace absorption spectroscopy (GFAAS) and was normalized to the protein content of each sample. We observed that C-2 is taken up 10 times more effectively than C-1 and over twice as effectively as C-3 in HEK293 cells and twice as effectively as C-1 and C-3 in HeLa cells (Figure S4, SI). To determine the abilities of the complexes to accumulate in the mitochondria, we treated HeLa cells with C-1, C-2, or C-3 (50 μM) in culture media for 24 h, and the mitochondria were isolated following modified literature procedures.[71−73] Both the mitochondrial and extramitochondrial fractions were analyzed for ruthenium content. Cells treated with C-1, C-2, or C-3 show 2−4 times greater uptake of ruthenium into the mitochondria compared to the rest of the cell, demonstrating the high selectivity of these compounds for the mitochondria (Figure S4, SI). Consistent with the cellular uptake studies, greater than 3-fold higher concentrations of C-2 are found in the mitochondria, compared to C-1 and C-3.

Encouraged by the high cell permeability and mitochondrial selectivity of C-2, we investigated the capability of this complex to inhibit MCU-mediated $_{m}Ca^{2+}$ uptake in intact, non-permeabilized cells. Briefly, HeLa cells were loaded with the cytosolic calcium concentration ($[Ca^{2+}]_c$) indicator Fluo-4 AM and the mitochondrial calcium concentration ($[Ca^{2+}]_m$) indicator Rhod-2 AM in the presence or absence of C-1, C-2, and C-3 (50 μM). Cells were stimulated with the GPCR agonist histamine (100 μM) to rapidly elevate $_{c}Ca^{2+}$ levels to induce $_{m}Ca^{2+}$ uptake.[74] Cells treated with C-2 showed significant inhibition of MCU-mediated $_{m}Ca^{2+}$ uptake compared to untreated cells (Figure 4A,B). These results were further confirmed using genetically encoded cytosolic (RGECO) and mitochondrial (GCamP6-mt) Ca^{2+} sensors (Figure 4C,D).[75,76] In contrast, intact cells treated with C-1 or C-3 did not show appreciable inhibition of $_{m}Ca^{2+}$ uptake. These results are consistent with our cell uptake and MCU Ca^{2+} uptake experiments, suggesting that C-2 is capable of inhibiting $_{m}Ca^{2+}$ uptake in intact cells as a result of its enhanced permeability compared to C-1 and C-3.

Having identified C-2 as a cell-permeable MCU inhibitor, we performed a dose−response analysis to determine the potency of this compound toward $_{m}Ca^{2+}$ uptake inhibition in a permeabilized cell system. Permeabilized HEK293T cells were treated with C-2 (1 nM to 1 μM). A 20 μM Ca^{2+} bolus was added after baseline recording, and the extramitochondrial calcium cleared was used as an indicator for MCU-mediated $_{m}Ca^{2+}$ uptake using Fura-2-FF (Figure 5A−C).[16] We found the 50% maximal inhibitory concentration (IC_{50}) for $_{m}Ca^{2+}$ uptake in permeabilized cells to be 2.6 nM for C-2, which is an order of magnitude more effective than commercially available Ru360 (IC_{50} = 30 nM) (Figure 5C). Furthermore, we observed complete inhibition of $_{m}Ca^{2+}$ uptake when cells were dosed with 10 nM C-2 while 500 nM of Ru360 was required for the same response (Figure 5A,B, and Figure S5, SI).

For C-2 to be an effective $_{m}Ca^{2+}$ uptake inhibitor, C-2 should selectively inhibit MCU-mediated Ca^{2+} uptake and not interact with other cellular ion channels. Despite showing greatly reduced $_{m}Ca^{2+}$ uptake, intact cells treated with C-2 showed normal cytosolic calcium dynamics when stimulated with histamine (Figure 5D,F). To further confirm the selectivity of C-2 for the MCU, we measured $_{m}Ca^{2+}$ uptake, $_{m}Ca^{2+}$ efflux rates, and matrix Ca^{2+} levels in permeabilized HEK293T cells before and after treatment with C-2 using the fluorescent Ca^{2+} indicator Fura-2-FF.[16] As expected, untreated cells displayed normal $[Ca^{2+}]_{out}$ clearance rates (Figure 5D). We next added Ru360 or C-2 to inhibit MCU-mediated Ca^{2+} uptake and subsequently visualized $[Ca^{2+}]_m$ efflux (Figure 5D). $[Ca^{2+}]_m$ efflux rates were similar between both inhibitors suggesting that Ru360 and C-2 selectively inhibit the MCU and do not affect $_{m}Ca^{2+}$ efflux channels (Figure 5E−G). To further confirm that C-2 did not affect mitochondrial calcium efflux, cells were treated with the sodium calcium exchanger (NCLX) inhibitor CGP-37157.[77] We observed no change in C-2 activity upon treatment with CGP-37157 and CCCP (Figure 5E−G). These results suggest that Ru360 and C-2 do not interact with other mitochondrial calcium transport proteins and selectively interact with the MCU.

Exploring the Mechanism of MCU Inhibition. Having observed the high potency of C-2 compared to Ru360, we next investigated its mechanism of action. Site-directed mutagenesis revealed that the serine residue S259 of the human MCU is required for maximum activity of Ru360. Mutating this serine residue to an alanine (S259A) renders partial resistance to Ru360-mediated MCU inhibition.[9] First, we tested if interaction with the S259 residue on the MCU is necessary for C-2 to be effective. HEK293T cells stably expressing Flag-tagged full-length human wild-type MCU (MCU^{WT}) or the mutant S259A (MCU^{S259A}) were permeabilized, and $_{m}Ca^{2+}$ uptake was measured as above. Cells expressing the MCU^{S259A} mutation displayed partial resistance to Ru360 inhibition of the MCU compared to MCU^{WT} cells (Figure 6B). In contrast, cells expressing the MCU^{S259A} mutation showed almost no change in the inhibitory activity of C-2 compared to the MCU^{WT} cells (Figure 6A). These results suggest that C-2 could inhibit the MCU in a manner distinct from Ru360.

A recent report revealed that the conserved human MCU cysteine residue C97 located in the MCU-NTD (residues 72−189)[26,27] in the mitochondrial matrix senses mitochondrial levels of reactive oxygen species and induces higher order oligomerization to regulate MCU channel activity (Figure 1).[74] Additionally, recent structural and biochemical studies have demonstrated the importance of the NTD in MCU oligomerization and activity.[20,21,27,74] To determine if C-2 interacts with the NTD, HEK293T cells stably expressing Flag-tagged full-length wild-type MCU (MCU^{WT}) and the mutant C97A (MCU^{C97A}) were permeabilized, and $_{m}Ca^{2+}$ uptake was measured as above. Upon MCU^{C97A} mutation, cells treated with C-2 showed significantly reduced MCU-inhibitory activity compared to MCU^{WT} cells (Figure 6C). In contrast, the MCU^{C97A} mutation had almost no effect on the activity of Ru360 (Figure 6D). Taken together, these studies suggest that C-2 and Ru360 may act on different regions of the MCU to inhibit mitochondrial calcium uptake.

To further elucidate the potential interaction of C-2 with the MCU-NTD, we investigated the interaction between C-2 and the uniformly ^{15}N-labeled recombinant human MCU-NTD (residues 72−189)[27] using solution nuclear magnetic resonance (NMR) spectroscopy. The $^{1}H-^{15}N$-heteronuclear single quantum coherence (HSQC) spectrum of the MCU-NTD in the absence of C-2 showed well-dispersed amide H(N) cross-peaks with homogeneous peak intensities, consistent with the well-folded and soluble domain (Figure 7A). Remarkably, upon addition of a 3-fold molar excess of C-2, the NMR sample showed a rapid formation of insoluble precipitate. A

DOI: 10.1021/acscentsci.8b00773
ACS Cent. Sci. 2019, 5, 153−166

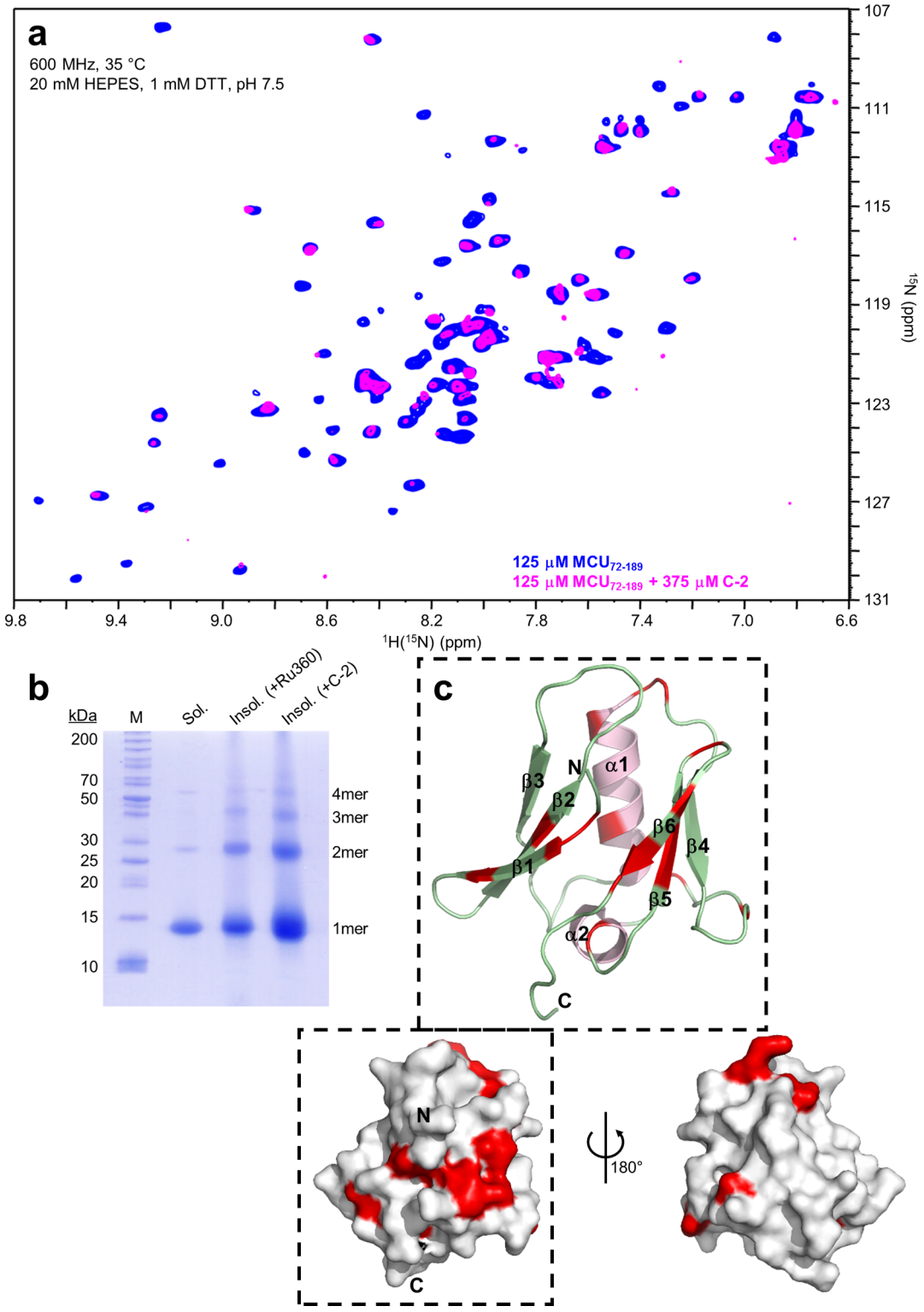

Figure 7. (A) $^{1}H-^{15}N$-heteronuclear single quantum coherence (HSQC) spectra of uniformly ^{15}N-labeled human MCU N-terminal domain (residues 72−189; MCU_{72-189}) in the absence (blue cross-peaks) and presence (magenta cross-peaks) of C-2. A large amount of the protein immediately precipitated out of solution with the addition of 3 molar excess C-2 to the sample with no detectable change in solvent pH or ionic strength. Consequently, most amide H(N) cross-peaks show a drastic loss in intensity compared to cross-peaks in the control spectrum. (B) Coomassie blue-stained 15% (w/v) SDS-PAGE gel visualizing the insoluble precipitate formed after mixing 125 μM MCU_{72-189} with 375 μM C-2 (Insol. + C-2) and 375 μM Ru360 (Insol. + Ru360) compared to untreated MCU_{72-189} protein (Sol.). (C) Cross-peak broadening map on the MCU_{72-189} high-resolution crystal structure (PDB 5KUJ).[27] Tentatively assigned residues which exhibited a ≥40% reduction in peak intensity are highlighted in red on the backbone ribbon view of MCU_{72-189} (top dashed box). The surface representation of the same view (bottom dashed box) shows that the most affected H(N) cross-peaks primarily cluster on one face of the domain.

DOI: 10.1021/acscentsci.8b00773
ACS Cent. Sci. 2019, 5, 153−166

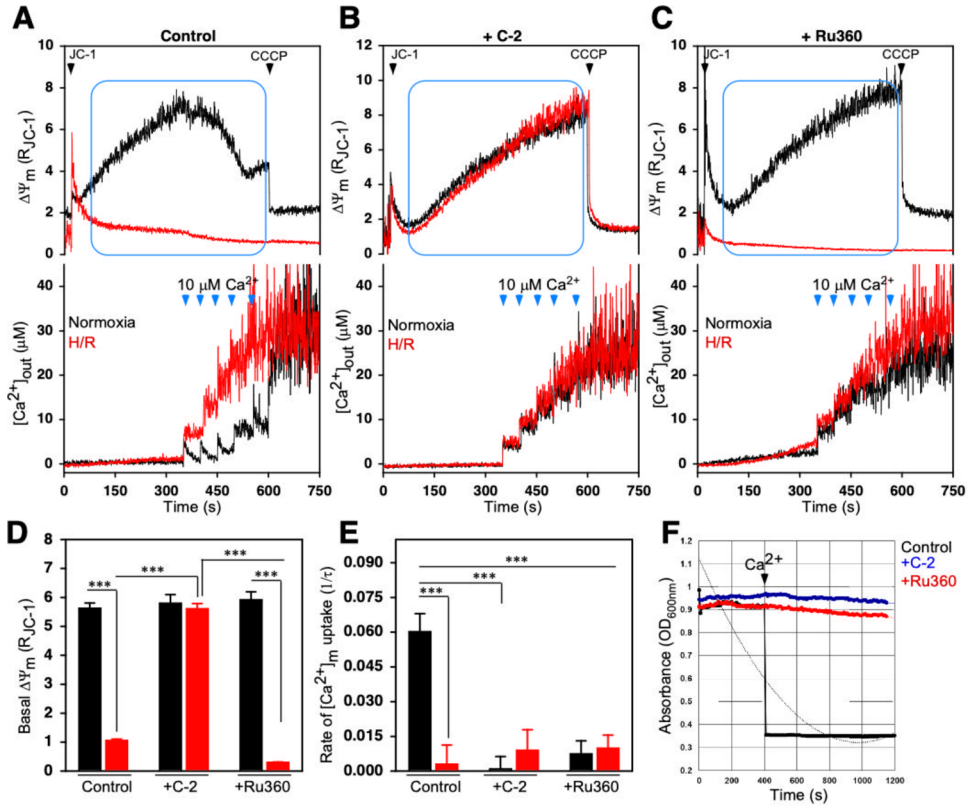

Figure 8. Measurement of $\Delta\Psi_m$ (top panels) and MCU-mediated Ca^{2+} uptake (bottom panels) in (A) control, (B) C-2, and (C) Ru360 treated NRVMs exposed to normoxia (black) and H/R (red). (D) Quantification of basal $\Delta\Psi_m$ from parts A−C under normoxia and H/R before the addition of extramitochondrial Ca^{2+} pulses. (E) Quantification of the rate of MCU-mediated Ca^{2+} uptake from parts A−C as a function of decrease in bath Ca^{2+} fluorescence. (F) Swelling of isolated NRVM mitochondria subjected to H/R injury in the absence (black trace) or presence (blue trace) of C-2 or Ru360 (red trace). Data represent mean ± SEM; ***$p < 0.001$; $n = 3–6$.

similar addition of C-2 to sample buffer alone showed neither precipitate formation nor a change in pH, suggesting that the insoluble aggregate contained MCU-NTD. Consistent with precipitation of the protein, the $^{1}H-^{15}N$-HSQC spectrum of the 1:3 MCU-NTD:C-2 sample mixture showed a drastic loss in most H(N) cross-peak intensities (Figure 7A). It is noteworthy that some of the remaining H(N) peaks of the protein also exhibited small chemical shift perturbations.

To determine if the MCU-NTD remained intact upon treatment with C-2, we resuspended the insoluble aggregate (Insol. + C-2) in loading dye and compared the migration of the protein to untreated, soluble MCU-NTD (Sol.) by SDS-PAGE analysis (Figure 7B). After Coomassie blue staining, the untreated MCU-NTD control showed clear bands indicating the presence of the monomer (~13.9 kDa) in addition to low levels of the dimer and tetramer oligomers which is characteristic of the native MCU-NTD conformation. The protein precipitate that formed upon treatment with C-2 showed a distinct and systematic laddering corresponding to the presence of monomer, dimer, trimer, tetramer, and higher aggregate formation. The appearance of the trimer and higher order aggregates upon treatment with C-2 may suggest that the MCU-NTD conformation induced by C-2 is different from that of the native conformation. Similar MCU-NTD aggregation was observed when the MCU-NTD was treated with lower molar ratios (i.e., 1:2 and 1:1) of C-2.

To distinguish whether C-2 induced a global or more local structural effect on the MCU-NTD, peaks exhibiting an intensity reduction of ≥40% were mapped (see the SI for details) onto the crystal structure of the domain (PDB 5KUJ).[27] Remarkably, these most severely affected H(N) cross-peaks were found to cluster close together on the two β-sheets of the β-grasp-like fold despite the long distance between these residues in sequence space (Figure 7C). The clustering of these perturbations could be a result of (i) direct binding with the compound, (ii) indirect effects of the lower soluble protein concentration shifting the self-association equilibrium, or (iii) C-2-mediated modifications to the protein. Nevertheless, these data collectively suggest that C-2 interacts with the MCU-NTD to induce aggregation of the protein and inhibit Ca^{2+} uptake through the MCU channel.[20−23,26,27] Notably, we have found that commercially available Ru360 also interacts with the purified MCU-NTD in a cell-free system, giving rise to precipitation and systematic laddering (Insol. + Ru360; Figure 7B). Given the structural similarity of Ru360 and C-2, it is not surprising that these compounds induce analogous conformational perturbations in the NTD of the MCU in solution. However, site-mutagenesis studies with MCU^{C97A} and MCU^{S259A} (Figure 6) clearly show that the inhibitory activity of C-2 is dependent on the mutation-status of the NTD, whereas the inhibitory activity of Ru360 is not. Thus, we hypothesize that the NTD is a potent target for MCU inhibition that is only accessible to C-2 because of its enhanced membrane permeability compared to Ru360.

Protection from Ca^{2+}-Induced PTP Opening and Hypoxia/Reoxygenation Injury. Given the Ca^{2+} uptake inhibiting properties and low toxicity of C-2, we hypothesized that C-2 could be used to protect cardiomyocytes from the

DOI: 10.1021/acscentsci.8b00773
ACS Cent. Sci. 2019, 5, 153−166

$_{m}Ca^{2+}$ overload that occurs during hypoxia/reoxygenation (H/R) injury and prevent mPTP opening and mitochondrial swelling.[34,37,78] Freshly isolated neonatal rat ventricular myocytes (NRVMs) treated with C-2 (50 μM) were subjected to 16 h of hypoxia (1% O_2−5% CO_2), followed by 8 h of reoxygenation (21% O_2−5% CO_2). Untreated NRVMs served as controls. After H/R injury, NRVMs were permeabilized and loaded with the JC-1 and Fura-FF to simultaneously measure $\Delta\Psi_m$ and $_{m}Ca^{2+}$ uptake.[16] Cells treated with C-2 maintained mitochondrial integrity with no loss of $\Delta\Psi_m$ after H/R injury (Figure 8B, top panel; and Figure 8D). Additionally, treatment with C-2 resulted in complete ablation of $_{m}Ca^{2+}$ uptake after H/R injury (Figure 8B, bottom panel; and 8E). On the contrary, untreated cells subjected to identical conditions showed no preservation of $\Delta\Psi_m$ and did not show normal $_{m}Ca^{2+}$ uptake (Figure 8A, top panel; and Figure 8D−E). In contrast to C-2, pretreatment with Ru360 did not prevent H/R-mediated $\Delta\Psi_m$ dissipation (Figure 8C−E). Additionally, we monitored the swelling of mitochondria isolated from NRVMs subjected to H/R injury in the absence (Figure 8F; black trace) or presence (Figure 8F; blue trace) of C-2 or Ru360 (Figure 8F; red trace). After baseline measurement of the absorbance at 600 nm, a single bolus of Ca^{2+} (250 μM) was added to induce mPTP opening. The decrease in mitochondrial absorbance indicates mitochondrial swelling and subsequent mPTP opening.[34] When cells were treated with C-2 or Ru360, we observed no decrease in absorbance after Ca^{2+} addition, indicating a lack of mitochondrial swelling (Figure 8F). These results demonstrate that inhibition of MCU-mediated $_{m}Ca^{2+}$ uptake by C-2 effectively prevents mPTP opening in response to H/R injury and when challenged with high Ca^{2+} concentrations.

DISCUSSION

Given the importance of $_{m}Ca^{2+}$ in mitochondrial bioenergetics, damage, and cell death, identification of effective MCU-mediated $_{m}Ca^{2+}$ uptake inhibitors has attracted considerable interest.[41,79−81] In this report, we describe the synthesis, characterization, and biological activity of a cell-permeable, highly potent, and selective MCU inhibitor. Identifying potent and selective MCU inhibitors has proven to be challenging, with reported potential inhibitors generally exhibiting low permeability or poor selectivity and mitochondrial targeting.[42] Given high potency and selectivity of Ru360, we focused our design on structurally related compounds. The syntheses of the oxo-bridged complexes Ru360 and C-1 are low-yielding and require tedious chromatographic purification.[56,57] In contrast, C-2, which we name Ru265, and C-3 can be prepared in moderate yields without the need for extensive purification. Additionally, the nitrido-bridged complexes can be accessed through the common starting material, $K_3[Ru_2(\mu\text{-}N)\text{-}Cl_8(OH_2)_2]$. This synthetic route allows for facile design of related analogues of Ru265 and C-3 through ligand substitution reactions. This straightforward chemical reaction is advantageous for studying structure−activity relationships to probe the biological activity of these complexes, which will be the focus of a future report.

Among the compounds studied, Ru265 showed the most effective MCU inhibition in nonpermeabilized cells. Furthermore, this compound is highly water-soluble (1 mg/mL) and exhibits low toxicity to human cells. The low toxicity of these complexes is significant because of the large number of known cytotoxic ruthenium compounds.[82−91] The minimal toxicity of Ru265 in contrast to many other ruthenium compounds highlights the importance of molecular structure and coordination geometry in the biological activity of metal-based compounds.[92−94] In our intact cellular models, Ru265 consistently inhibited MCU-mediated $_{m}Ca^{2+}$ uptake without any effect on intracellular Ca^{2+} dynamics.

A series of recent reports have definitively elucidated the structure of the full-length MCU through cryo-EM and X-ray crystallographic techniques.[20−23] Most notably, these reports highlight the assembly of the NTD directly under the channel pore in the mitochondrial matrix. Our binding studies suggest that Ru265 interacts with the MCU-NTD and may perturb the assembly of NTD through aggregation, inhibiting normal channel function (Figure 7). Based on these data, it is tempting to speculate that the Ru265-dependent aggregation of the NTD could inhibit the dynamics of the NTD and immediately adjacent coiled−coiled domains required to regulate pore opening and closing. Our speculation is supported by the lack of rapid MCU Ca^{2+} uptake inhibition at lower Ru265 concentrations (Figure 5). It remains to be definitively determined whether Ru265-induced NTD aggregation regulates the Ca^{2+} binding and release mechanism; this study will be detailed in a future report. Alternatively, binding of Ru265 to the NTD could modulate MCU channel activity by promoting conformations which constrict the pore.

We have previously shown that human MCU-NTD contains a contiguous electronegative surface patch which can bind divalent cations and inhibit the MCU channel function via a shift of the self-association equilibrium of the domain toward monomer formation.[27] Given the charge, symmetry, and size of Ru265, it is possible that Ru265 also interacts with the MRAP of the MCU-NTD, with the ability to bridge MCU-NTD subunits. Using Ru265, we observed a robust inhibition of the MCU channel, which may be a consequence of the higher order oligomerization of the MCU-NTD that it induces. In the context of the full-length MCU, the bridging of dimers could prevent MCU-NTD dimer dynamics proposed to be involved in MCU gating by locking the domains in an assembly pattern, promoting a closed pore and inhibited Ca^{2+} uptake. Future high-resolution structural investigations using the full-length human protein are required to determine the precise structural mechanism by which Ru265 causes MCU inhibition.

In summary, the current study presents a ruthenium-based complex that not only inhibits the MCU selectively in vitro but also efficiently inhibits MCU activity and prevents mitochondrial membrane potential dissipation, mitochondrial swelling, and mPTP opening in cells exposed to simulated ischemic reperfusion injury. We show that Ru265 is over 10 times more effective at inhibiting $_{m}Ca^{2+}$ uptake than Ru360, and potentially interacts with the matrix side of the MCU rather than the intermembrane Ca^{2+} binding sites. Furthermore, Ru265 inhibits MCU activity without disrupting normal cellular Ca^{2+} dynamics. This work presents a new class of compounds that have important implications in drug development strategies for diseases that are intimately associated with mitochondrial dysfunction.

ASSOCIATED CONTENT

Supporting Information

The Supporting Information is available free of charge on the ACS Publications website at DOI: 10.1021/acscentsci.8b00773.

DOI: 10.1021/acscentsci.8b00773
ACS Cent. Sci. 2019, 5, 153−166

Experimental details, complex characterization data, cell viability curves, cell uptake, UV−vis spectra, and dose−response data for Ca^{2+} uptake inhibition (PDF)
X-ray crystal data for C-2 and C-3 (CIF)

AUTHOR INFORMATION

Corresponding Authors

*E-mail: jjw275@cornell.edu.
*E-mail: muniswamy@uthscsa.edu.

ORCID

Joshua J. Woods: 0000-0002-6213-4093
Justin J. Wilson: 0000-0002-4086-7982

Author Contributions

[∇]J. J. Woods and N. Nemani contributed equally. J. J. Woods, N. Nemani, S. Shanmughapriya, A. Kumar, S. R. Nathan, M. Zhang, M. Thomas, E. Carvalho, P. B. Stathopulos, J. J. Wilson, and M. Madesh performed and analyzed experiments involving chemical synthesis, biochemical, mitochondrial bioenergetics, and molecular and cellular experiments. J. J. Wilson, P. B. Stathopulos, and M. Madesh conceived, designed, analyzed, and interpreted experimental data. J. J. Woods, N. Nemani, P. B. Stathopulos, J. J. Wilson, and M. Madesh wrote the manuscript with contributions from S. Shanmughapriya and A. Kumar.

Notes

The authors declare no competing financial interest.

ACKNOWLEDGMENTS

This research in the laboratory of M. Madesh was funded by the National Institutes of Health (R01GM109882, R01HL086699, R01HL142673, R01HL119306). Research in the laboratory of J. J. Wilson was supported by the National Science Foundation (NSF) (CHE-1750295). S. Shanmughapriya is supported by the NIH K99/R00 grant (1 K99 HL138268-01). E. Carvalho and N. Nemani are supported by the AHA fellowships (18POST33990217 and 17PRE33660720). J. J. Woods is supported by the NSF-GRFP (DGE-1650441). This work made use of the Cornell NMR facility, which is funded in part by the NSF (CHE-1531632). We thank Reggie Jacob for helpful comments on the manuscript and Samantha Davalos for assistance in preparing the artwork associated with this manuscript.

REFERENCES

(1) Berridge, M. J.; Bootman, M. D.; Roderick, H. L. Calcium Signalling: Dynamics, Homeostasis and Remodelling. *Nat. Rev. Mol. Cell Biol.* **2003**, *4*, 517−529.
(2) Soboloff, J.; Rothberg, B. S.; Madesh, M.; Gill, D. L. STIM Proteins: Dynamic Calcium Signal Transducers. *Nat. Rev. Mol. Cell Biol.* **2012**, *13*, 549−565.
(3) Clapham, D. E. Calcium Signaling. *Cell* **2007**, *131*, 1047−1058.
(4) Hogan, P. G.; Lewis, R. S.; Rao, A. Molecular Basis of Calcium Signaling in Lymphocytes: STIM and ORAI. *Annu. Rev. Immunol.* **2010**, *28*, 491−533.
(5) Kirichok, Y.; Krapivinsky, G.; Clapham, D. E. The Mitochondrial Calcium Uniporter is a Highly Selective Ion Channel. *Nature* **2004**, *427*, 360−364.
(6) Kamer, K. J.; Mootha, V. K. The Molecular Era of the Mitochondrial Calcium Uniporter. *Nat. Rev. Mol. Cell Biol.* **2015**, *16*, 545−553.
(7) Rizzuto, R.; De Stefani, D.; Raffaello, A.; Mammucari, C. Mitochondria as Sensors and Regulators of Calcium Signalling. *Nat. Rev. Mol. Cell Biol.* **2012**, *13*, 566−578.
(8) Nemani, N.; Shanmughapriya, S.; Madesh, M. Molecular Regulation of MCU: Implications in Physiology and Disease. *Cell Calcium* **2018**, *74*, 86−93.
(9) Baughman, J. M.; Perocchi, F.; Girgis, H. S.; Plovanich, M.; Belcher-Timme, C. A.; Sancak, Y.; Bao, X. R.; Strittmatter, L.; Goldberger, O.; Bogorad, R. L.; Koteliansky, V.; Mootha, V. K. Integrative Genomics Identifies MCU as an Essential Component of the Mitochondrial Calcium Uniporter. *Nature* **2011**, *476*, 341−345.
(10) De Stefani, D.; Raffaello, A.; Teardo, E.; Szabò, I.; Rizzuto, R. A Forty-Kilodalton Protein of the Inner Membrane is the Mitochondrial Calcium Uniporter. *Nature* **2011**, *476*, 336−340.
(11) Mallilankaraman, K.; Doonan, P.; Cárdenas, C.; Chandramoorthy, H. C.; Müller, M.; Miller, R.; Hoffman, N. E.; Gandhirajan, R. K.; Molgó, J.; Birnbaum, M. J.; Rothberg, B. S.; Mak, D. O. D.; Foskett, J. K.; Madesh, M. MICU1 is an Essential Gatekeeper for MCU-Mediated Mitochondrial Ca^{2+} Uptake That Regulates Cell Survival. *Cell* **2012**, *151*, 630−644.
(12) Sancak, Y.; Markhard, A. L.; Kitami, T.; Kovacs-Bogdan, E.; Kamer, K. J.; Udeshi, N. D.; Carr, S. A.; Chaudhuri, D.; Clapham, D. E.; Li, A. A.; Calvo, S. E.; Goldberger, O.; Mootha, V. K. EMRE is an Essential Component of the Mitochondrial Calcium Uniporter Complex. *Science* **2013**, *342*, 1379−1382.
(13) Perocchi, F.; Gohil, V. M.; Girgis, H. S.; Bao, X. R.; McCombs, J. E.; Palmer, A. E.; Mootha, V. K. MICU1 Encodes a Mitochondrial EF Hand Protein Required for Ca^{2+} uptake. *Nature* **2010**, *467*, 291−296.
(14) Plovanich, M.; Bogorad, R. L.; Sancak, Y.; Kamer, K. J.; Strittmatter, L.; Li, A. A.; Girgis, H. S.; Kuchimanchi, S.; De Groot, J.; Speciner, L.; Taneja, N.; OShea, J.; Koteliansky, V.; Mootha, V. K. MICU2, a Paralog of MICU1, Resides within the Mitochondrial Uniporter Complex to Regulate Calcium Handling. *PLoS One* **2013**, *8*, e55785.
(15) Csordás, G.; Golenár, T.; Seifert, E. L.; Kamer, K. J.; Sancak, Y.; Perocchi, F.; Moffat, C.; Weaver, D.; De la Fuente, S.; Bogorad, R.; Koteliansky, V.; Adijanto, J.; Mootha, V. K.; Hajnóczky, G. MICU1 Controls Both the Threshold and Cooperative Activation of the Mitochondrial Ca^{2+} Uniporter. *Cell Metab.* **2013**, *17*, 976−987.
(16) Mallilankaraman, K.; Cárdenas, C.; Doonan, P. J.; Chandramoorthy, H. C.; Irrinki, K. M.; Golenár, T.; Csordás, G.; Madireddi, P.; Yang, J.; Müller, M.; Miller, R.; Kolesar, J. E.; Molgó, J.; Kaufman, B.; Hajnóczky, G.; Foskett, J. K.; Madesh, M. MCUR1 is an Essential Component of Mitochondrial Ca^{2+} Uptake that Regulates Cellular Metabolism. *Nat. Cell Biol.* **2012**, *14*, 1336−1343.
(17) Patron, M.; Checchetto, V.; Raffaello, A.; Teardo, E.; VecellioReane, D.; Mantoan, M.; Granatiero, V.; Szabò, I.; DeStefani, D.; Rizzuto, R. MICU1 and MICU2 Finely Tune the Mitochondrial Ca^{2+} Uniporter by Exerting Opposite Effects on MCU Activity. *Mol. Cell* **2014**, *53*, 726−737.
(18) Oxenoid, K.; Dong, Y.; Cao, C.; Cui, T.; Sancak, Y.; Markhard, A. L.; Grabarek, Z.; Kong, L.; Liu, Z.; Ouyang, B.; Cong, Y.; Mootha, V. K.; Chou, J. J. Architecture of the Mitochondrial Calcium Uniporter. *Nature* **2016**, *533*, 269−273.
(19) Bick, A. G.; Calvo, S. E.; Mootha, V. K. Evolutionary Diversity of the Mitochondrial Calcium Uniporter. *Science* **2012**, *336*, 886.
(20) Baradaran, R.; Wang, C.; Siliciano, A. F.; Long, S. B. Cryo-EM Structures of Fungal and Metazoan Mitochondrial Calcium Uniporters. *Nature* **2018**, *559*, 580−584.
(21) Fan, C.; Fan, M.; Orlando, B. J.; Fastman, N. M.; Zhang, J.; Xu, Y.; Chambers, M. G.; Xu, X.; Perry, K.; Liao, M.; Feng, L. X-Ray and Cryo-EM Structures of the Mitochondrial Calcium Uniporter. *Nature* **2018**, *559*, 575−579.
(22) Nguyen, N. X.; Armache, J. P.; Lee, C.; Yang, Y.; Zeng, W.; Mootha, V. K.; Cheng, Y.; Bai, X.; Jiang, Y. Cryo-EM Structure of a Fungal Mitochondrial Calcium Uniporter. *Nature* **2018**, *559*, 570−574.
(23) Yoo, J.; Wu, M.; Yin, Y.; Herzik, M. A.; Lander, G. C.; Lee, S.-Y. Cryo-EM Structure of a Mitochondrial Calcium Uniporter. *Science* **2018**, *361*, 506−511.

DOI: 10.1021/acscentsci.8b00773
ACS Cent. Sci. 2019, 5, 153−166

(24) Hoffman, N. E.; Chandramoorthy, H. C.; Shamugapriya, S.; Zhang, X.; Rajan, S.; Mallilankaraman, K.; Gandhirajan, R. K.; Vagnozzi, R. J.; Ferrer, L. M.; Sreekrishnanilayam, K.; Natarajaseenivasan, K.; Vallem, S.; Force, T.; Choi, E. T.; Cheung, J. Y.; Madesh, M. MICU1 Motifs Define Mitochondrial Calcium Uniporter Binding and Activity. *Cell Rep.* **2013**, *5*, 1576−1588.
(25) Petrungaro, C.; Zimmermann, K. M.; Küttner, V.; Fischer, M.; Dengjel, J.; Bogeski, I.; Riemer, J. The Ca^{2+}-Dependent Release of the Mia40-Induced MICU1-MICU2 Dimer from MCU Regulates Mitochondrial Ca^{2+} Uptake. *Cell Metab.* **2015**, *22*, 721−733.
(26) Lee, Y.; Min, C. K.; Kim, T. G.; Song, H. K.; Lim, Y.; Kim, D.; Shin, K.; Kang, M.; Kang, J. Y.; Youn, H.-S.; Lee, J.-G.; An, J. Y.; Park, K. R.; Lim, J. J.; Kim, J. H.; Kim, J. H.; Park, Z. Y.; Kim, Y.-S.; Wang, J.; Kim, D. H.; Eom, S. H. Structure and Function of the N-Terminal Domain of the Human Mitochondrial Calcium Uniporter. *EMBO Rep.* **2015**, *16*, 1318−1333.
(27) Lee, S. K.; Shanmughapriya, S.; Mok, M. C. Y.; Dong, Z.; Tomar, D.; Carvalho, E.; Rajan, S.; Junop, M. S.; Madesh, M.; Stathopulos, P. B. Structural Insights into Mitochondrial Calcium Uniporter Regulation by Divalent Cations. *Cell Chem. Biol.* **2016**, *23*, 1157−1169.
(28) Tomar, D.; Dong, Z.; Shanmughapriya, S.; Koch, D. A.; Thomas, T.; Hoffman, N. E.; Timbalia, S. A.; Goldman, S. J.; Breves, S. L.; Corbally, D. P.; Nemani, N.; Fairweather, J. P.; Cutri, A. R.; Zhang, X.; Song, J.; Jaña, F.; Huang, J.; Barrero, C.; Rabinowitz, J. E.; Luongo, T. S.; Schumacher, S. M.; Rockman, M. E.; Dietrich, A.; Merali, S.; Caplan, J.; Stathopulos, P. B.; Ahima, R. S.; Cheung, J. Y.; Houser, S. R.; Koch, W. J.; Patel, V.; Gohil, V. M.; Elrod, J. W.; Rajan, S.; Madesh, M. MCUR1 is a Scaffold Factor for the MCU Complex Function and Promotes Mitochondrial Bioenergetics. *Cell Rep.* **2016**, *15*, 1673−1685.
(29) Gunter, T. E.; Gunter, K. K.; Sheu, S.-S.; Gavin, C. E. Mitochondrial Calcium Transport: Physiological and Pathological Relevance. *Am. J. Physiol.* **1994**, *267*, C313−319.
(30) Hajnóczky, G.; Robb-Gaspers, L. D.; Seitz, M. B.; Thomas, A. P. Decoding of Cytosolic Calcium Oscillations in the Mitochondria. *Cell* **1995**, *82*, 415−424.
(31) Denton, R.; McCormack, J. G. Ca^{2+} as a Second Messenger Within Mitochondria Of The Heart And Other Tissues. *Annu. Rev. Physiol.* **1990**, *52*, 451−466.
(32) Santo-Domingo, J.; Demaurex, N. Calcium Uptake Mechanisms of Mitochondria. *Biochim. Biophys. Acta, Bioenerg.* **2010**, *1797*, 907−912.
(33) Bernardi, P. Mitochondrial Transport of Cations: Channels, Exchangers, and Permeability Transition. *Physiol. Rev.* **1999**, *79*, 1127−1155.
(34) Shanmughapriya, S.; Rajan, S.; Hoffman, N. E.; Higgins, A. M.; Tomar, D.; Nemani, N.; Hines, K. J.; Smith, D. J.; Eguchi, A.; Vallem, S.; Shaikh, F.; Cheung, M.; Leonard, N. J.; Stolakis, R. S.; Wolfers, M. P.; Ibetti, J.; Chuprun, J. K.; Jog, N. R.; Houser, S. R.; Koch, W. J.; Elrod, J. W.; Madesh, M. SPG7 is an Essential and Conserved Component of the Mitochondrial Permeability Transition Pore. *Mol. Cell* **2015**, *60*, 47−62.
(35) Orrenius, S.; Zhivotovsky, B.; Nicotera, P. Regulation of Cell Death: The Calcium-Apoptosis Link. *Nat. Rev. Mol. Cell Biol.* **2003**, *4*, 552−565.
(36) De Stefani, D.; Rizzuto, R.; Pozzan, T. Enjoy the Trip: Calcium in Mitochondria Back and Forth. *Annu. Rev. Biochem.* **2016**, *85*, 161−192.
(37) Marchi, S.; Pinton, P. The Mitochondrial Calcium Uniporter Complex: Molecular Components, Structure and Physiopathological Implications. *J. Physiol.* **2014**, *592*, 829−839.
(38) Luongo, T. S.; Lambert, J. P.; Yuan, A.; Zhang, X.; Gross, P.; Song, J.; Shanmughapriya, S.; Gao, E.; Jain, M.; Houser, S. R.; Koch, W. J.; Cheung, J. Y.; Madesh, M.; Elrod, J. W. The Mitochondrial Calcium Uniporter Matches Energetic Supply with Cardiac Workload during Stress and Modulates Permeability Transition. *Cell Rep.* **2015**, *12*, 23−34.
(39) Kwong, J. Q.; Lu, X.; Correll, R. N.; Schwanekamp, J. A.; Vagnozzi, R. J.; Sargent, M. A.; York, A. J.; Zhang, J.; Bers, D. M.; Molkentin, J. D. The Mitochondrial Calcium Uniporter Selectively Matches Metabolic Output to Acute Contractile Stress in the Heart. *Cell Rep.* **2015**, *12*, 15−22.
(40) Medvedeva, Y. V.; Weiss, J. H.; Weiss, J. H.; Medvedeva, Y. V. Intramitochondrial Zn^{2+} Accumulation via the Ca^{2+} Uniporter Contributes to Acute Ischemic Neurodegeneration. *Neurobiol. Dis.* **2014**, *68*, 137−144.
(41) Giorgi, C.; Agnoletto, C.; Bononi, A.; Bonora, M.; De Marchi, E.; Marchi, S.; Missiroli, S.; Patergnani, S.; Poletti, F.; Rimessi, A.; Suski, J. M.; Wieckowski, M. R.; Pinton, P. Mitochondrial Calcium Homeostasis as Potential Target for Mitochondrial Medicine. *Mitochondrion* **2012**, *12*, 77−85.
(42) Arduino, D. M.; Wettmarshausen, J.; Vais, H.; Navas-Navarro, P.; Cheng, Y.; Leimpek, A.; Ma, Z.; Delrio-Lorenzo, A.; Giordano, A.; Garcia-Perez, C.; Médard, G.; Kuster, B.; García-Sancho, J.; Mokranjac, D.; Foskett, J. K.; Alonso, M. T.; Perocchi, F. Systematic Identification of MCU Modulators by Orthogonal Interspecies Chemical Screening. *Mol. Cell* **2017**, *67*, 711−723.
(43) Kon, N.; Murakoshi, M.; Isobe, A.; Kagechika, K.; Miyoshi, N.; Nagayama, T. DS16570511 is a Small-Molecule Inhibitor of the Mitochondrial Calcium Uniporter. *Cell Death Discov.* **2017**, *3*, 17045.
(44) Thu, V. T.; Kim, H. K.; Long, L. T.; Lee, S. R.; Hanh, T. M.; Ko, T. H.; Heo, H. J.; Kim, N.; Kim, S. H.; Ko, K. S.; Rhee, B. D.; Han, J. NecroX-5 Prevents Hypoxia/Reoxygenation Injury by Inhibiting the Mitochondrial Calcium Uniporter. *Cardiovasc. Res.* **2012**, *94*, 342−350.
(45) Antonenko, Y. N.; Rokitskaya, T. I.; Cooper, A. J. L.; Krasnikov, B. F. Minocycline Chelates Ca^{2+}, Binds to Membranes, and Depolarizes Mitochondria by Formation of Ca^{2+}-Dependent Ion Channels. *J. Bioenerg. Biomembr.* **2010**, *42*, 151−163.
(46) Santo-Domingo, J.; Vay, L.; Hernández-Sanmiguel, E.; Lobatón, C. D.; Moreno, A.; Montero, M.; Alvarez, J. The Plasma Membrane Na^{+}/Ca^{2+} Exchange Inhibitor KB-R7943 is Also a Potent Inhibitor of the Mitochondrial Ca^{2+} Uniporter. *Br. J. Pharmacol.* **2007**, *151*, 647−654.
(47) Kapuscinski, J.; Darzynkiewicz, Z. Interactions of Antitumor Agents Ametantrone and Mitoxantrone (Novatrone) with Double-Stranded DNA. *Biochem. Pharmacol.* **1985**, *34*, 4203−4213.
(48) Mazerski, J.; Martelli, S.; Borowski, E. The Geometry of Intercalation Complex of Antitumor Mitoxantrone and Ametantrone with DNA: Molecular Dynamics Simulations. *Acta Biochim. Polym.* **1998**, *45*, 1−11.
(49) Boland, M. P.; Fitzgerald, K. A.; O'Neill, L. A. J. Topoisomerase II Is Required for Mitoxantrone to Signal Nuclear Factor KB Activation in HL60 Cells. *J. Biol. Chem.* **2000**, *275*, 25231−25238.
(50) Smith, P. J.; Morgan, S. A.; Fox, M. E.; Watson, J. V. Mitoxantrone-DNA Binding and the Induction of Topoisomerase II Associated DNA Damage in Multi-Drug Resistant Small Cell Lung Cancer Cells. *Biochem. Pharmacol.* **1990**, *40*, 2069−2078.
(51) Nägele, H.; Castel, M. A.; Deutsch, O.; Wagner, F. M.; Reichenspurner, H. Heart Transplantation in a Patient with Multiple Sclerosis and Mitoxantrone-Induced Cardiomyopathy. *J. Heart Lung Transplant.* **2004**, *23*, 641−643.
(52) Goebel, M.; Kaplan, E. Anthracycline-Induced Cardiotoxicity − A Review. *Oncol. Res. Treat.* **2004**, *15*, 198−204.
(53) Ying, W.-L.; Emerson, J.; Clarke, M. J.; Sanadi, D. R. Inhibition of Mitochondrial Calcium Ion Transport by an Oxo-Bridged Dinuclear Ruthenium Ammine Complex. *Biochemistry* **1991**, *30*, 4949−4952.
(54) Matlib, M. A.; Zhou, Z.; Knight, S.; Ahmed, S.; Choi, K. M.; Krause-Bauer, J.; Phillips, R.; Altschuld, R.; Katsube, Y.; Sperelakis, N.; Bers, D. M. Oxygen-Bridged Dinuclear Ruthenium Amine Complex Specifically Inhibits Ca^{2+} Uptake into Mitochondria in Vitro and in Situ in Single Cardiac Myocytes. *J. Biol. Chem.* **1998**, *273*, 10223−10231.
(55) Emerson, J.; Clarke, M. J.; Ying, W. L.; Sanadi, D. R. The Component of "Ruthenium Red" Responsible for Inhibition of

DOI: 10.1021/acscentsci.8b00773
ACS Cent. Sci. 2019, 5, 153−166

Mitochondrial Calcium Ion Transport. Spectra, Electrochemistry, and Aquation Kinetics. Crystal Structure of μ-O-$[(HCO)_2(NH_3)_4Ru]_2Cl_3$. *J. Am. Chem. Soc.* **1993**, *115*, 11799−11805.
(56) Nathan, S. R.; Pino, N. W.; Arduino, D. M.; Perocchi, F.; MacMillan, S. N.; Wilson, J. J. Synthetic Methods for the Preparation of a Functional Analogue of Ru360, a Potent Inhibitor of Mitochondrial Calcium Uptake. *Inorg. Chem.* **2017**, *56*, 3123−3126.
(57) Nathan, S. R.; Wilson, J. J. Synthesis and Evaluation of a Ruthenium-Based Mitochondrial Calcium Uptake Inhibitor. *J. Visualized Exp.* **2017**, *128*, e56527.
(58) Cao, C.; Wang, S.; Cui, T.; Su, X.-C.; Chou, J. J. Ion and Inhibitor Binding of the Double-Ring Ion Selectivity Filter of the Mitochondrial Calcium Uniporter. *Proc. Natl. Acad. Sci. U. S. A.* **2017**, *114*, E2846−E2851.
(59) Gushchin, A. L.; Laricheva, Y. A.; Abramov, P. A.; Sokolov, M. N.; Abramov, P. A. Synthesis and Electrochemical Properties of $[Ru^{IV}_2O(PhCN)_4Cl_6]$. *Inorg. Chem. Commun.* **2018**, *95*, 1387−7003.
(60) Urgiles, J.; Nathan, S. R.; MacMillan, S. N.; Wilson, J. J. Dinuclear Nitrido-Bridged Ruthenium Complexes Bearing Diimine Ligands. *Dalton Trans.* **2017**, *46*, 14256−14263.
(61) Dunitz, J. D.; Orgel, L. E. Application of Molecular-Orbital Theory to Some Binuclear Coordination Compounds. *J. Chem. Soc.* **1953**, 2594−2596.
(62) Cleare, M. J.; Griffith, W. P. Binuclear Nitrido-Complexes of Ruthenium. *Chem. Commun.* **1968**, *21*, 1302.
(63) Griffith, W. P.; McManus, N. T.; Skapski, A. C. X-Ray Crystal Structure of $[Ru_2N(ethylenediamine)_5]Cl_5\cdot H_2O$; a Novel Complex Containing Both Nitrido and Ethylenediamine Bridges. *J. Chem. Soc., Chem. Commun.* **1984**, *7*, 434.
(64) Ng, H.-Y.; Cheung, W.-M.; Kwan Huang, E.; Wong, K.-L.; Sung, H. H.-Y.; Williams, I. D.; Leung, W.-H. Ruthenium Chalcogenonitrosyl and Bridged Nitrido Complexes Containing Chelating Sulfur and Oxygen Ligands. *Dalton Trans.* **2015**, *44*, 18459−18468.
(65) Ciechanowicz, M.; Skapski, A. C. Crystal Structure of Potassium μ-Nitrido-Bis[Aquotetrachlororuthenate(IV)]. *J. Chem. Soc. A* **1971**, *84*, 1792−1794.
(66) Freshney, R. I. *Culture of Animal Cells*, 5th ed.; John Wiley & Sons, Inc.: Hoboken, NJ, 2005.
(67) Shanmughapriya, S.; Rajan, S.; Hoffman, N. E.; Zhang, X.; Guo, S.; Kolesar, J. E.; Hines, K. J.; Ragheb, J.; Jog, N. R.; Caricchio, R.; Baba, Y.; Zhou, Y.; Kaufman, B. A.; Cheung, J. Y.; Kurosaki, T.; Gill, D. L.; Madesh, M. Ca^{2+} Signals Regulate Mitochondrial Metabolism by Stimulating CREB-Mediated Expression of the Mitochondrial Ca^{2+} Uniporter Gene MCU. *Sci. Signaling* **2015**, *8*, ra23.
(68) Reers, M.; Smith, T. W.; Chen, L. B. J-aggregate formation of a carbocyanine as a quantitative fluorescent indicator of membrane potential. *Biochemistry* **1991**, *30*, 4480−4486.
(69) King, A. P.; Gellineau, H. A.; Ahn, J. E.; MacMillan, S. N.; Wilson, J. J. Bis(Thiosemicarbazone) Complexes of Cobalt(III). Synthesis, Characterization, and Anticancer Potential. *Inorg. Chem.* **2017**, *56*, 6609−6623.
(70) Egger, A. E.; Rappel, C.; Jakupec, M. A.; Hartinger, C. G.; Heffeter, P.; Keppler, B. K. Development of an Experimental Protocol for Uptake Studies of Metal Compounds in Adherent Tumor Cells. *J. Anal. At. Spectrom.* **2009**, *24*, 51−61.
(71) Komor, A. C.; Schneider, C. J.; Weidmann, A. G.; Barton, J. K. Cell-Selective Biological Activity of Rhodium Metalloinsertors Correlates with Subcellular Localization. *J. Am. Chem. Soc.* **2012**, *134*, 19223−19233.
(72) Boyle, K. M.; Barton, J. K. A Family of Rhodium Complexes with Selective Toxicity toward Mismatch Repair-Deficient Cancers. *J. Am. Chem. Soc.* **2018**, *140*, 5612−5624.
(73) Ahmad, K. A.; Iskandar, K. B.; Hirpara, J. L.; Clement, M. V.; Pervaiz, S. Hydrogen Peroxide-Mediated Cytosolic Acidification is a Signal for Mitochondrial Translocation of Bax during Drug-Induced Apoptosis of Tumor Cells. *Cancer Res.* **2004**, *64*, 7867−7878.
(74) Dong, Z.; Shanmughapriya, S.; Tomar, D.; Siddiqui, N.; Lynch, S.; Nemani, N.; Breves, S. L.; Zhang, X.; Tripathi, A.; Palaniappan, P.; Riitano, M. F.; Worth, A. M.; Seelam, A.; Carvalho, E.; Subbiah, R.; Jaña, F.; Soboloff, J.; Peng, Y.; Cheung, J. Y.; Joseph, S. K.; Caplan, J.; Rajan, S.; Stathopulos, P. B.; Madesh, M. Mitochondrial Ca^{2+} Uniporter is a Mitochondrial Luminal Redox Sensor That Augments MCU Channel Activity. *Mol. Cell* **2017**, *65*, 1014−1028.
(75) Zhao, Y.; Araki, S.; Wu, J.; Teramoto, T.; Chang, Y.-F.; Nakano, M.; Abdelfattah, A. S.; Fujiwara, M.; Ishihara, T.; Nagai, T.; Campbell, R. E. An Expanded Palette of Genetically Encoded Ca^{2+} Indicators. *Science* **2011**, *333*, 1888−1891.
(76) Nakai, J.; Ohkura, M.; Imoto, K. A High Signal-to-Noise Ca^{2+} Probe Composed of a Single Green Fluorescent Protein. *Nat. Biotechnol.* **2001**, *19*, 137−141.
(77) Chiesi, M.; Schwaller, R.; Eichenberger, K. Structural Dependency of the Inhibitory Action of Benzodiazepines and Related Compounds on the Mitochondrial Na^+-Ca^{2+} Exchanger. *Biochem. Pharmacol.* **1988**, *37*, 4399−4403.
(78) Luongo, T. S.; Lambert, J. P.; Gross, P.; Nwokedi, M.; Lombardi, A. A.; Shanmughapriya, S.; Carpenter, A. C.; Kolmetzky, D.; Gao, E.; van Berlo, J. H.; Tsai, E. J.; Molkentin, J. D.; Chen, X.; Madesh, M.; Houser, S. R.; Elrod, J. W. The Mitochondrial Na^+/Ca^{2+} Exchanger is Essential for Ca^{2+} Homeostasis and Viability. *Nature* **2017**, *545*, 93−97.
(79) Storey, N. M.; Lambert, D. G. Mitochondrial Pharmacology Turns Its Sights on the Ca^{2+} Uniporter. *Cell Death Discov.* **2017**, *3*, 17064.
(80) Sebag, S. C.; Koval, O. M.; Paschke, J. D.; Winters, C. J.; Comellas, A. P.; Grumbach, I. M. Inhibition of the Mitochondrial Calcium Uniporter Prevents IL-13 and Allergen-Mediated Airway Epithelial Apoptosis and Loss of Barrier Function. *Exp. Cell Res.* **2018**, *362*, 400−411.
(81) Xie, N.; Wu, C.; Wang, C.; Cheng, X.; Zhang, L.; Zhang, H.; Lian, Y. Inhibition of the Mitochondrial Calcium Uniporter Inhibits Aβ-Induced Apoptosis by Reducing Reactive Oxygen Species-Mediated Endoplasmic Reticulum Stress in Cultured Microglia. *Brain Res.* **2017**, *1676*, 100−106.
(82) Alessio, E. Thirty Years of the Drug Candidate NAMI-A and the Myths in the Field of Ruthenium Anticancer Compounds: A Personal Perspective. *Eur. J. Inorg. Chem.* **2017**, *2017*, 1549−1560.
(83) Wachter, E.; Heidary, D. K.; Howerton, B. S.; Parkin, S.; Glazer, E. C. Light-Activated Ruthenium Complexes Photobind DNA and are Cytotoxic in the Photodynamic Therapy Window. *Chem. Commun.* **2012**, *48*, 9649−9651.
(84) Han Ang, W.; Dyson, P. J. Classical and Non-Classical Ruthenium-Based Anticancer Drugs: Towards Targeted Chemotherapy. *Eur. J. Inorg. Chem.* **2006**, *2006*, 4003−4018.
(85) Süss-Fink, G. Areneruthenium Complexes as Anticancer Agents. *Dalton Trans.* **2010**, *39*, 1673−1688.
(86) Wang, F.; Chen, H.; Parsons, S.; Oswald, I. D. H.; Davidson, J. E.; Sadler, P. J. Kinetics of Aquation and Anation of Ruthenium(II) Arene Anticancer Complexes, Acidity and X-Ray Structures of Aqua Adducts. *Chem. - Eur. J.* **2003**, *9*, 5810−5820.
(87) Hartinger, C. G.; Jakupec, M. A.; Zorbas-Seifried, S.; Groessl, M.; Egger, A.; Berger, W.; Zorbas, H.; Dyson, P. J.; Keppler, B. K. KP1019, A New Redox-Active Anticancer Agent - Preclinical Development and Results of a Clinical Phase I Study in Tumor Patients. *Chem. Biodiversity* **2008**, *5*, 2140−2155.
(88) Peacock, A. F. A.; Habtemariam, A.; Fernández, R.; Walland, V.; Fabbiani, F. P. A.; Parsons, S.; Aird, R. E.; Jodrell, D. I.; Sadler, P. J. Tuning the Reactivity of Osmium(II) and Ruthenium(II) Arene Complexes under Physiological Conditions. *J. Am. Chem. Soc.* **2006**, *128*, 1739−1748.
(89) Mühlgassner, G.; Bartel, C.; Schmid, W. F.; Jakupec, M. A.; Arion, V. B.; Keppler, B. K. Biological Activity of Ruthenium and Osmium Arene Complexes with Modified Paullones in Human Cancer Cells. *J. Inorg. Biochem.* **2012**, *116*, 180−187.
(90) Lameijer, L. N.; Ernst, D.; Hopkins, S. L.; Meijer, M. S.; Askes, S. H. C.; Le Dévédec, S. E.; Bonnet, S. A Red-Light-Activated Ruthenium-Caged NAMPT Inhibitor Remains Phototoxic in Hypoxic Cancer Cells. *Angew. Chem., Int. Ed.* **2017**, *56*, 11549−11553.

DOI: 10.1021/acscentsci.8b00773
ACS Cent. Sci. 2019, 5, 153−166

(91) Dutta, B.; Scolaro, C.; Scopelliti, R.; Dyson, P. J.; Severin, K. Importance of the π-Ligand: Remarkable Effect of the Cyclopentadienyl Ring on the Cytotoxicity of Ruthenium PTA Compounds. *Organometallics* **2008**, *27*, 1355−1357.
(92) Allardyce, C. S.; Dyson, P. J. Metal-Based Drugs that Break the Rules. *Dalton Trans.* **2016**, *45*, 3201−3209.
(93) Kilpin, K. J.; Dyson, P. J. Enzyme Inhibition by Metal Complexes: Concepts, Strategies and Applications. *Chem. Sci.* **2013**, *4*, 1410−1419.
(94) Barry, N. P. E.; Sadler, P. J. Exploration of the Medical Periodic Table: Towards New Targets. *Chem. Commun.* **2013**, *49*, 5106−5131.

DOI: 10.1021/acscentsci.8b00773
ACS Cent. Sci. 2019, 5, 153−166